Autonomous docking of a feeder vessel

B.J. de Kruif

MARIN, Maritime Research Institute Netherlands. Email: b.j.d.kruif@marin.nl

Synopsis

Autonomous sailing is seen as one of the possible solutions to cope with the decrease in qualified personnel, to minimise the risk to humans and ships in challenging conditions, and to decrease the environmental impact of the transport sector. Autonomous sailing is not limited to moving the vessel safely through the seas, but it also includes docking the vessel. A feeder vessel that distributes cargo spends a relative large percentage of its time on (un)docking, compared to a seafaring cargo vessel. Automating this part of the operation might further save on resources.

The objective of this work is to automatically approach a dock for an underactuated vessel. It comprises the design of a time-dependent trajectory, as well as a controller that can track this trajectory. The solution is tailored for our 71m long feeder vessel designed for the EU-H2020 Moses project. The focus is on approaching the dock from cruising speed until the speed of the vessel is near-zero. The result of the study is a high-fidelity time simulation that shows the behaviour of the vessel in combination with the control system when it approaches a dock. From these simulations it can be concluded that the ship can approach the dock with only azimuthing thrusters to a speed when the bow thrusters become effective. The then fully actuated vessel might be safely docked with a dynamical positioning system.

Keywords: Automatic docking; Underactuated control systems; Trajectory tracking; Marine systems

1 Introduction

Autonomous sailing is seen as one of the possible solutions to cope with the decrease in qualified personnel, to minimise the risk to humans and ships in challenging conditions, and to decrease the environmental impact of the transport sector. Autonomous sailing is not limited to moving the vessel safely through the seas, but it also includes docking the vessel. Feeders vessels collect shipping containers from different ports and transport them to central container terminals where they are loaded to bigger vessels, or vice versa. Such vessels spend a relative large percentage of its time on (un)docking compared to a seafaring cargo vessel: the distance travelled between the deep water port and smaller ports is smaller than between the deep water ports. Automating this part of the operation, therefore, can save on resources.

The objective of this work is to automatically approach a dock. The focus is on approaching the dock from cruising speed until the speed of the vessel is near-zero and the dynamical positioning system can take over. This is deemed the most critical part of the docking manoeuvre as the ship has to decelerate and steer without bow thrusters and hence is underactuated, i. e. has less actuators than degrees of freedom. The design comprises the design of a time-dependent trajectory, as well as a controller that can track this trajectory. The solution is tailored for our 71m long feeder vessel designed for the EU-H2020 Moses project. The vessel has two azimuthing thrusters and a bow thruster. The ship used in this study is shown in Figure 1.

In section 2 a time dependent trajectory to the dock is treated. The optimal path to approach a dock can be determined as an Optimal Control Problem (Okazaki and Ohtsu, 2008; Mizuno et al., 2015). However, solving an OCP is computationally demanding and might be difficult in real-time applications. This problem can be circumvented by solving the optimal trajectory beforehand for many initial situations, and use machine learning to interpolate between them (Okazaki and Ohtsu, 2008; Ahmed and Hasegawa, 2015), or use a Bézier curve to describe the path (Sawada et al., 2021). In De Kruif (2022) it has been shown that Bézier curves can be used to generate smooth trajectories and the corresponding time derivatives. The acceleration and rate-of-turn values are limited when the trajectory is not too challenging, but must be checked afterwards. The results will be treated concisely for the convenience of the reader.

A control model is needed for our control design. A simulation model based on manoeuvring coefficients is available in a simulation environment (Yasukawa and Yoshimura, 2015). The manoeuvring coefficients were determined by CFD calculations. This simulation model is too complex to base a controller on, so a control model is deduced from it. Since we want to follow a track in the plane, we are not so much interested in the heading as we are in the course. Hence the model considered is a Nomoto model with side slip (Sonnenburg and Woolsey, 2012). The surge-velocity dependent model is treated in section 3.

An underactuated controller is designed in section 4 based on this control model. The generated trajectory from section 2 provides a (x, y)-position and an orientation, but at cruising speeds the bow thrusters of the ship are not

Authors' Biographies

B.J. de Kruif is employed at the Maritime Research Institute Netherlands as researcher in the field of control. His research activities focus on controlling ship motions for autonomous surface and underwater vessels.

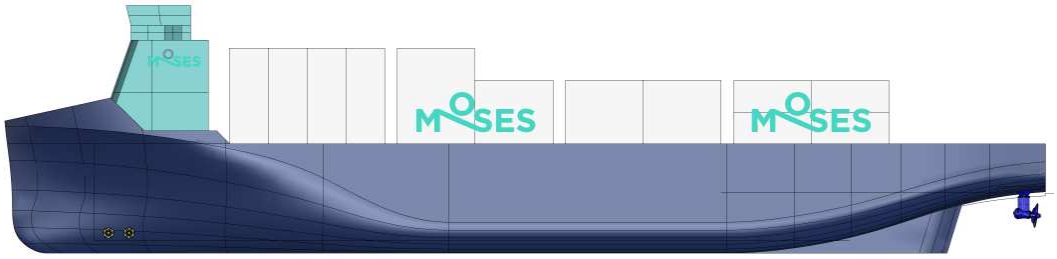

Figure 1: Feeder vessel used in this study

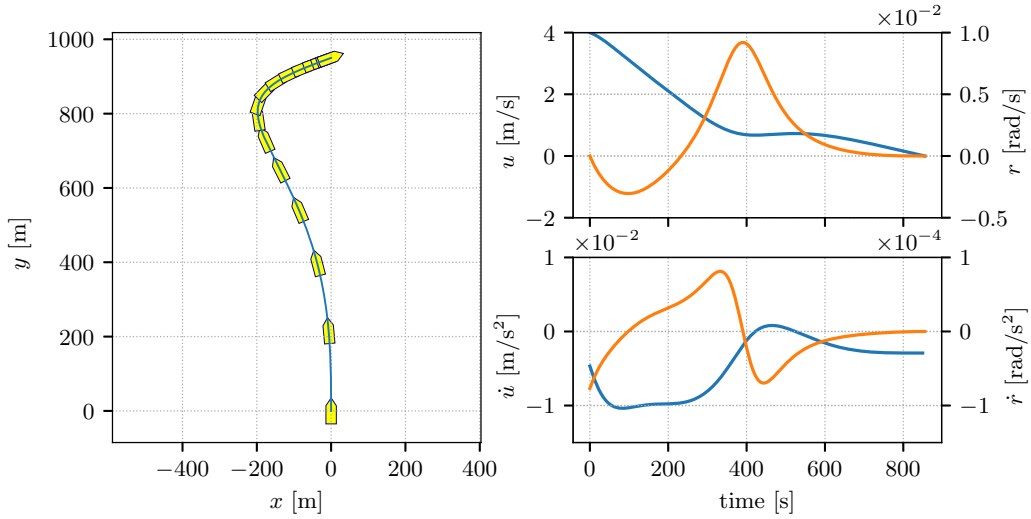

Figure 2: Generated Bézier trajectory. The left-hand plot shows the path, while the right-hand plots show the velocities and accelerations. In these, the blue lines are related to the surge-velocity, and the orange line are related to the rate-of-turn.

available, and we can only control two of the three degrees of freedom. The position can be directly controlled, as shown in (Berge et al., 1998; Lefeber et al., 2003), in which the heading is free. Alternatively, the required position is translated to a speed and course which are then controlled (Breivik, 2010). The latter of these options is chosen, as this gives more control on the actual heading during the approaching phase. When the switch to a dynamic positioning controller occurs at low speeds, then the heading should only get by corrected a limited amount. The designed controller is tested on the detailed simulation platform to evaluate its performance in section 5. The results are elaborated upon in the same section. Conclusions are drawn in section 6.

2 Trajectory generation

Before the approach to the dock is started, the vessel is assumed to be sailing from waypoint to waypoint. When the ship is at a distance of around 13 ship lengths, which is slightly above 900 meters for our feeder vessel, the approaching phase is initiated (De Kruif, 2022). At this position, a fifth order Bézier curve is constructed that starts at the switching position, and ends at the required position close to the dock. The heading and rate of turn at the initial position are set to the current heading and to zero respectively. The heading at the final position is set to 20 degrees with respect to the dock. This is done to avoid a possible collision with the dock due to waves, and to minimise the suction between the ship and the dock. The final rate-of-turn is set at zero degrees per second.

The resulting Bézier curve is a path in space only, and is dependent on its path parameter $0 \leq s \leq 1$. A relation between the path variable and time makes the path a time-dependent trajectory. If we relate the path variable to time as $s = t/T(2 - t/T)$, in which t denotes time, T the duration to traverse the path, then the duration of the approaching phase is fully determined by the initial velocity and by the path parameters. Furthermore, the final velocity is guaranteed to be zero. Refer for more information to the above cited reference. With the path parameters and the dependency of the path variable on the time, the trajectory and its time derivatives are fully determined. An example trajectory is shown in Figure 2.

Table 1: Values identified for the three parts of the control model. The right most two column indicate the poles and zeros for the linearised transfer function.

model	parameter	value	pole/zero	value
rate of turn	α	$-8.47\ 10^5 \cdot u$	$p_{r=0}$	$9.27\ 10^{-3} \cdot u$
	β	$4.84\ 10^9/u$		
	K/T	$1.09\ 10^{-8}$		
course	a	$9.784\ 10^{-3} \cdot u$	p	$-9.78\ 10^{-3} \cdot u$
	b	-0.512	z_1	$-7.62\ 10^{-3} \cdot u$
	c	$-10.1/u$	z_2	$3.19\ 10^{-2} \cdot u$
speed	$m - X_{\dot{u}}$	$3.3\ 10^6$		
	X_{uu}	-1506		

3 Ship motion model

A detailed numeric model based on manoeuvring coefficients is available in our simulation environment (MARIN, 2022). This simulation model is the basis of the a control model. An alteration that has been made to the detailed numeric model, is to replace the azimuthing thrusters with a force actuator. To mimic the underactuated behaviour during the approaching phase, the force actuator is located between the azimuthing thrusters and can only generate a force in lateral and longitudinal direction. An allocation algorithm that converts this force to settings for the azimuthing thruster is not yet present and will be included in future work. The bow thruster is not available during the approaching phase, and is therefore not included in the model.

The identification of the course of the ship due to the forces is done in two steps. First a rate-of-turn is identified as a result of lateral forces, and then the course is identified as a result of the rate-of-turn. The speed and course model are assumed uncoupled.

3.1 Rate-of-turn model

The ship used in this study is course unstable. This behaviour can be described by a first order Nomoto model (Nomoto, 1972):

$$\dot{r} = -\frac{K}{T}(\alpha + \beta r^2)r + \frac{K}{T}F_y, \tag{1}$$

where the rudder angle has been replaced by the lateral force F_y. In this equation r denotes the rate-of-turn, and $\alpha < 0, \beta > 0, K/T > 0$ are parameters to be determined. The values of α, β can be found by fitting them on a Bech's reverse spiral, while the value of K/T is found by the step response around the $F_y = 0$ N equilibrium.

The results of the identification simulations are shown in Figure 3. Figure 3(a) shows the relation between the rate-of-turn and the lateral force. The hysteresis loop of the course unstable ship is clearly visible. Running the simulation for different fixed surge velocities results in a set of curves. The top of Figure 3(b) shows the fit of the Bech's reverse spiral with the parameters α, β for $u = 2.5$ m/s. The grey line is from the simulation, the orange line is the fit. The values of α, β, and other values, are presented in Table 1. Both α and β are speed dependent.

The bottom part of Figure 3(b) shows the response to step changes on the lateral force at the equilibrium $F_y = 0$ N with a solid grey line. The dashed line shows the 63% change from the minimum to the maximim amplitude from which the time constant of the first order system is deduced. When this time constant is used to estimate the response at $t = 1500$ seconds, then the orange line is found. For velocities below 1 m/s a first order model does not adequately describe the response.

The linearised transfer function for $r = 0$ rad/s is found as:

$$\frac{r}{F_y} = \frac{K/T}{s + \alpha K/T}. \tag{2}$$

The pole corresponding to the linearised system is given in the table and shows the unstable behaviour of the system at this operating point. The location of the pole changes to the other side of the imaginary axis if we linearise around a higher rate-of-turn.

3.2 Course model

The relation between the course and the rate-of-turn is based on the work of (Sonnenburg and Woolsey, 2012):

$$\dot{\chi} = -a\chi + a\psi + (1+b)\dot{\psi} + c\ddot{\psi} \rightarrow \dot{\kappa} = -a\kappa + b\dot{\psi} + c\ddot{\psi}, \tag{3}$$

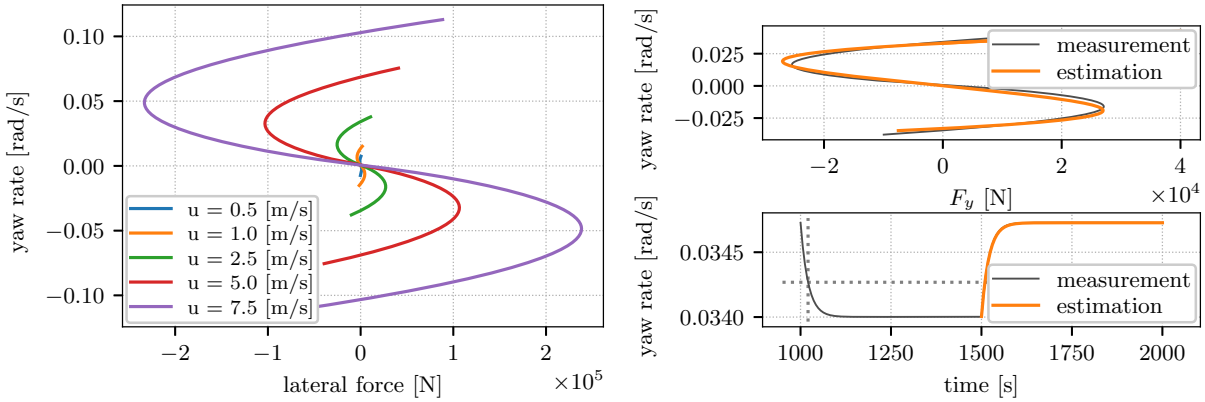

(a) Bech's reverse spiral test.

(b) fit of the simulations at $u = 2.5$m/s.

Figure 3: Identification of the rate-of-turn model from a detailed numerical model.

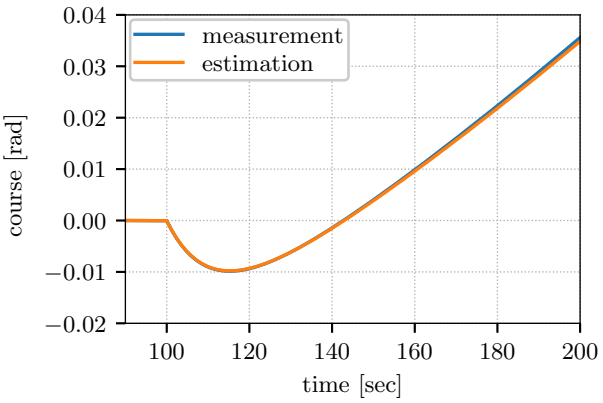

Figure 4: The course with fixed surge speed $u = 0.5$ m/s and a step on the reference rate-of-turn.

in which χ denotes the course, ψ the heading and $\kappa = \chi - \psi$ the slip angle. In the cited reference the parameter $c \equiv 0$. However, if we apply a lateral force, the vessel will move to the side first, and only when it has rotated, then the surge speed will change the course to the other direction. At lower speeds, this effect is significant. This non-minimum phase behaviour is caught when $c \neq 0$.

The values of the parameters were identified in a closed loop simulation in which the rate-of-turn was controlled. A series of steps was given as reference to the rate-of-turn, and by means of a least squares fit the relation between the slip angle and rate-of-turn in (3) was calculated. The values are again shown in Table 1. Figure 4 shows the course when the rate-of-turn reference value is changed at $t = 100$ sec. The non-minimum phase behaviour of the course due to the lateral force is clearly present at this low velocity. The simulation and the approximation are nearly on top of each other for this velocity. The transfer function of (3) is calculated as:

$$\frac{\chi}{r} = \frac{cs^2 + (1+b)s + a}{s(s+a)} = \frac{(\tau_{z_1} s + 1)(\tau_{z_2} s + 1)}{s(\tau_p s + 1)} \tag{4}$$

in which we have used the knowledge that the transfer from heading to course is equal to one when sailing straight, i.e. when $s = 0$, to come to the right-hand side expression. The locations of the poles and zeros are the inverses of the time constants τ and are found through straightforward algebra. Their values are given in Table 1. The second zero is in the right-hand plane and it approaches the imaginary axis for low speed. This zero limits the bandwidth of a course controller.

3.3 Speed model

The manoeuvring model for the surge speed, with the hydrodynamic cross coupling removed, is given as:

$$(m - X_{\dot{u}})\dot{u} = mvr + X_{u|u|}u|u| + F_x, \tag{5}$$

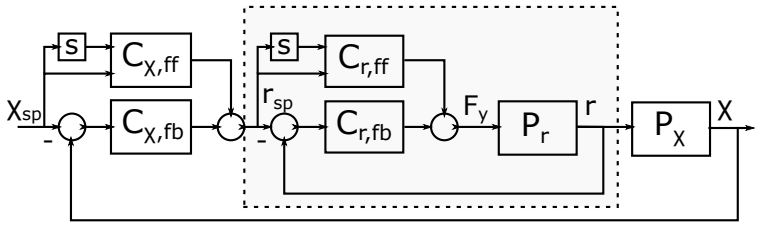

Figure 5: Control setup for the course. The course setpoint, $\chi_{\rm sp}$, results from the CB algorithm. The speed controller is independent of the course controller.The 's' denotes a differentiation in the Laplace domain. The other blocks are treated in the text.

where m gives the rigid body mass, $X_{\dot{u}}$ the added mass, u, v, r are the velocities in surge, sway and yaw direction, and F_x the applied longitudinal force. The parameter values are given in Table 1.

4 Control

The vessel should track the time-dependent earth-fixed trajectory described in section 2. Before a controller is designed, these positions are transformed to a speed and a course by a Constant Bearing (CB) algorithm (Breivik, 2010).

4.1 Constant bearing algorithm

The velocity vector that the vessel should track is given by CB as:

$$v_{\rm d} = v_{\rm t} + v_{\rm a} = v_{\rm t} + \gamma \frac{\tilde{p}}{||\tilde{p}||}, \text{ with } \tilde{p} = p_{\rm t} - p. \tag{6}$$

In this equation, $v_{\rm d}$ is the desired velocity vector, and is composed of the target velocity vector provided by the trajectory, $v_{\rm t}$, and a velocity that brings the true vessel in the direction of current position of the trajectory, $v_{\rm a}$. The position is denoted by p. The speed and course of the vessel can then be obtained as:

$$U = ||v_d||_2, \qquad \chi = \arctan\left(v_{d,y}/v_{d,x}\right). \tag{7}$$

The value of γ results from the distance between the target position and the actual vessel position:

$$\gamma = U_{\rm max} \frac{\sqrt{\tilde{p}^T \tilde{p}}}{\sqrt{(\tilde{p}^T \tilde{p} + \Delta^2)}}. \tag{8}$$

The parameter $U_{\rm max}$ is the maximum speed by which actual vessel is moving toward the target point, and Δ the distance at which it is halved. $U_{\rm max}$ should be smaller than the minimal target velocity, otherwise the desired velocity can change sign, which results in large changes in the course. The value of Δ is increased until a smooth operation is obtained.

4.2 Cascaded course control

The controller to keep course is designed as a cascade controller. This approach is used as the non-linearities and the unstable pole of the inner loop can be addressed first. The resulting inner loop then becomes stable, which allows for a simple design for the outer loop. A single loop compensator with an unstable zero and pole would otherwise lead to a high sensitivity peak (Skogestad and Postlethwaite, 2007). An overview of the cascade controller with the system model described in section 3 is shown in Figure 5. The elements of the figure will be treated next.

4.2.1 Rate-of-turn controller

The rate-of-turn controller is built from a feedback controller and a feed forward controller. The feed forward controller calculates the lateral force based on the set point for the rate-of-turn, while the feedback controller should compensate for deviations. The feed forward signal can be calculated directly from (1):

$$C_{r,\rm ff} = \alpha r_{\rm sp} + \beta r_{\rm sp}^3 + \frac{T}{K} \dot{r}_{\rm sp}. \tag{9}$$

In this, and following equations, the subscript 'sp' indicates the set point value. The feedback controller is based on (2). When the loop is closed with $C_{r,\mathrm{fb}} = K_\mathrm{d}$, we obtain the transfer function:

$$\frac{r}{F_y} = \frac{K_\mathrm{d} K/T}{s + K/T(\alpha + K_\mathrm{d})}. \tag{10}$$

A feedback gain $K_\mathrm{d} > -\alpha$ will stabilise this system, as also found in (Neuffer and Owens, 1992). With this stabilised inner loop, the outer loop is designed.

4.2.2 Course controller

The linear transfer function from the required rate-of-turn to the course is a series connection of (4) and (10):

$$\frac{\chi}{r_\mathrm{sp}} = \frac{(\tau_{z_1} s + 1)(\tau_{z_2} s + 1)}{s(\tau_p s + 1)} \frac{K_\mathrm{d} K/T}{s + K/T(\alpha + K_\mathrm{d})} \tag{11}$$

If we design our feedback controller to cancel the pole at τ_p and the stable zero τ_{z_1} and use a gain of K_p to close the loop:

$$C_{\chi,\mathrm{fb}} = K_\mathrm{p} \frac{\tau_p s + 1}{\tau_{z_1} s + 1}, \tag{12}$$

then we get the characteristic equation:

$$f(s) = s^2 + s\left(K/T(\alpha + K_\mathrm{d}) + \tau_{z_2} K_\mathrm{p} K_\mathrm{d} K/T\right) + K_\mathrm{p} K_\mathrm{d} K/T \tag{13}$$

The poles are selected such that the system mimics a second order system with natural frequency ω_n and relative damping ζ, if the gains are selected as:

$$K_\mathrm{d} = \omega_\mathrm{n}(T/K)(2\zeta - \tau_{z_2}\omega_\mathrm{n}) - \alpha, \tag{14}$$

$$K_\mathrm{p} = (T/K)(\omega_n^2/K_\mathrm{d}). \tag{15}$$

The value of K_d should be larger than $-\alpha$ to stabilise the inner loop. We select $\omega_\mathrm{n} = -1/\tau_{z_2}$, and in general we set $\zeta > 0.8$. Since we relate the bandwidth to the location of right half plane zero, we decrease the bandwidth for lower velocities. This is needed, as this zero poses a fundamental bound on the bandwidth.

The feed forward controller is the stable part of the inverse of the transfer between from the required rate to the course:

$$C_{\chi,\mathrm{ff}} = \frac{s(\tau_p s + 1)}{\tau_{z_1} s + 1}. \tag{16}$$

Note that this transfer function is not proper, but as we have access to the analytic time derivatives of the reference signal, it can be implemented.

4.3 Speed controller

The linearised system of (5) is an open integrator. A single feedback gain is used as feedback controller. Integral action could be used, but this would be advantageous for constant speeds, which will not occur during the approaching phase. The forces due to the required acceleration and damping are fed forward.

5 Results

A simulation is performed with in-house developed commercially available simulation software (MARIN, 2022). The manoeuvring coefficients are obtained from CFD calculations in which the free surface effects were ignored due to the low speed. As we are testing the ability to follow a continuous track, no external disturbances are included. The force calculated by the controller is directly applied at the mean position of the azimuthing pods.

The identified parameters were used in the feed forward controller. The bandwidth of the course feedback controller is scaled with the surge velocity, although it is capped at a maximum of $\omega_\mathrm{n} = 0.2$ rad/s. In order to avoid overshoot, a relative damping of $\zeta = 1$ is used. The maximum velocity with which the vessel approaches the target vessel is used to select the value for the parameter $U_\mathrm{max} = 0.5$ m/s. As argued before, this value should be lower than the expected speed of the target vessel. At this speed, the bow thrusters would be effective, and the controller would become fully actuated. The value $\Delta = 15$ is found by increasing its value until we got a smooth motion to the target position. The static feedback gain for the speed controller is set to $K = 10^5$, which results in a closed loop bandwidth of $\omega = 0.03$ rad/s.

Some results of the simulation are shown in Figure 6. The same trajectory as shown in Figure 2 is used. This trajectory is shown with the dotted grey line. Figure 6(a) shows the vessel path as well as the reference path. The

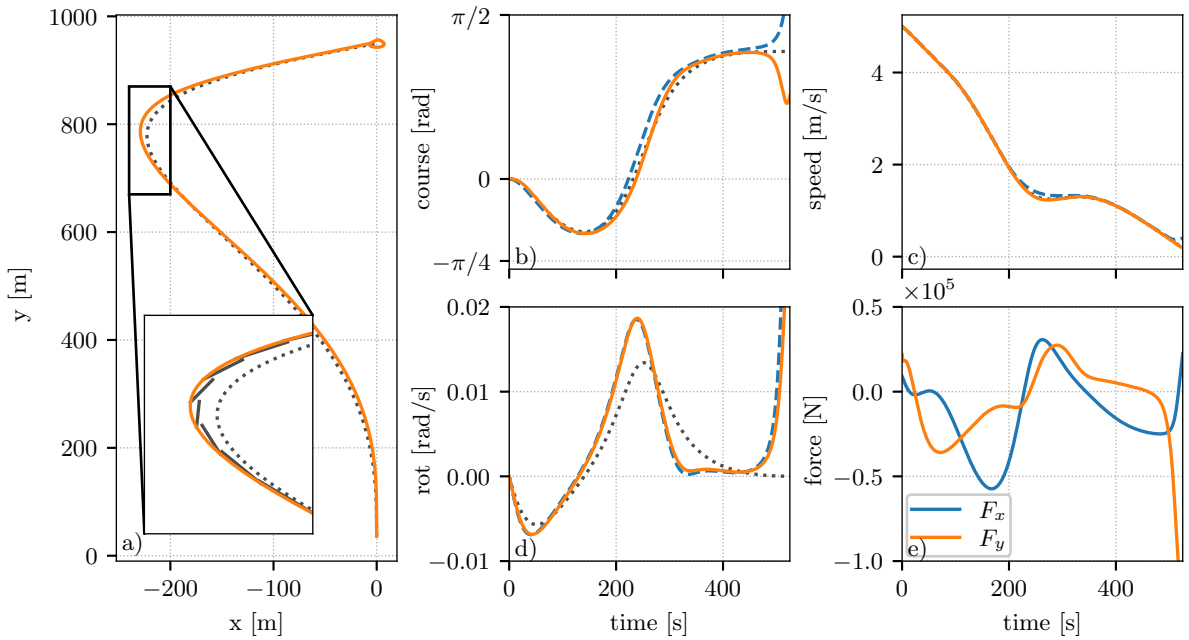

Figure 6: Simulation showing the approach to the dock of the underactuated feeder vessel. The dotted lines indicate the original Bézier trajectory, the dashed lines the output of the CB algorithm and the solid lines are the simulated responses.

maximum track error, emphasised at the zoom-inset, is approximately 10 m. In this part of the trajectory there is a large curvature with a surge speed above 1.25 m/s. As we are controlling the course, and not the heading, the vessel has a sway velocity here, and hence is drifting. This part of the trajectory should take place on a safe distance from the dock. In the inset the black lines indicate the target velocities that stem from the CB algorithm. It shows that the required velocity direction is not only targeted to minimise the current cross track error, but also incorporated the actual trajectory velocity. This is the reason why CB is used instead of a more path based approach such as a Line of Sight approach.

At the end of the simulation run one can observe that the course is no longer tracked. The velocity at this position is near zero, $u < 0.5$ m/s. At this velocity the manoeuvrability of the craft is very low, and as the trajectory velocity is lower than the maximum approach velocity, the sign coming from the CB algorithm can quickly change. This is not deemed a problem, as the bow thrusters will be available at velocities around 1 m/s and the ship can be controlled as a fully actuated ship. Even so, the vessel stays close to the end point of the run in Figure 6(a).

The course is depicted in Figure 6(b), while the rate of turn in shown in Figure 6(d). The dotted line in (d) gives the *course-rate* calculated by the Bézier trajectory, while the dashed and solid line show the *yaw-rate*. Their relation is provided by (3). This again shows that the vessel is drifting in this region. At the end of the run the tracking error becomes large. While the rate-of-turn goes to a positive value, the course is initially going down. This is the non-minimum phase behaviour. Although not shown in the graph, the course increases slightly later. In combination with the constant value for $U_{\max}$ in the CB, the underactuated controller is not able to track the course at these very low velocities.

Figure 6(c) shows the tracking of the speed. The maximum error found is approximately 0.2 m/s. The control is done for the fast majority by the feed forward controller. Figure 6(e) shows the requested forces. Around $t \approx 250$ seconds the longitudinal and lateral forces change direction. This indicate that the azimuthing thrusters need to rotate to the other direction. This is a point of attention for the allocation algorithm.

Although a dynamical model has been identified and used as feed forward controller, there still are errors between the reference and the response. This indicates that the feed forward is not flawless. The identification for the course behaviour is done at constant fixed velocity, while this is not true for the simulation. Furthermore, at lower speeds, the low order model fits the data worse. Which of these, or another effect, is dominant has to be further investigated.

6 Conclusions

In this study a controller is designed and tested for an underactuated course unstable feeder vessel. In order to do this, an available high fidelity model is simplified such that it could be used for control design. A smooth trajectory that brings the vessel from the current position and orientation close to the dock could be tracked. As the controller is designed as a cascade controller, intermediate signals have a clear interpretation which should help when the docking is tested on a scaled ship in our basins.

In the next steps of the research, it is recommended to incorporate disturbances to the ship such as wind and wave effects, and to include the allocation from force to azimuthing angles and RPMs. With those included, a better indication of the limitations of the approach can be achieved. Furthermore, the current underactuated controller works well to approximately 0.5 m/s. To actually dock, the ship has to arrive at lower speeds. The control architecture needs to be extended such that the bow thruster is used at these low velocities to keep the vessel under tight control.

Acknowledgement

MOSES project has received funding from the European Union's Horizon 2020 research & innovation programme under grant agreement No. 861678. Content reflects only the authors' view and the Agency is not responsible for any use that may be made of the information it contains.

References

Ahmed, Y., Hasegawa, K., 2015. Consistently Trained Artificial Neural Network for Automatic Ship Berthing Control. TransNav, the International Journal on Marine Navigation and Safety of Sea Transportation 9, 417–426.

Berge, S.P., Ohtsu, K., Fossen, T.I., 1998. Nonlinear Control of Ships Minimizing the Position Tracking Errors. IFAC Proceedings Volumes 31, 129–134.

Breivik, M., 2010. Topics in Guided Motion Control of Marine Vehicles. Ph.D. thesis. Norwegian University of Science and Technology.

De Kruif, B.J., 2022. Applied path planning for feeder vessel docking, in: 14th IFAC Conference on Control Applications in Marine Systems, Robotics and Vehicles, IFAC, Kongens Lyngby, Danmark.

Lefeber, E., Pettersen, K., Nijmeijer, H., 2003. Tracking control of an underactuated ship. IEEE Transactions on Control Systems Technology 11, 52–61.

MARIN, 2022. aNySIM XMF. URL: `https://www.marin.nl/en/facilities-and-tools/software/anysim`.

Mizuno, N., Uchida, Y., Okazaki, T., 2015. Quasi Real-Time Optimal Control Scheme for Automatic Berthing. IFAC-PapersOnLine 48, 305–312.

Neuffer, D., Owens, D.H., 1992. Global stabilization of unstable ship dynamics using PD control. Proceedings of the IEEE Conference on Decision and Control , 519–520.

Nomoto, K., 1972. Paper 1. Problems and Requirements of Directional Stability and Control of Surface Ships. Journal of Mechanical Engineering Science 14, 1–5.

Okazaki, T., Ohtsu, K., 2008. A study on ship berthing support system - Minimum time berthing control -, in: 2008 IEEE International Conference on Systems, Man and Cybernetics, IEEE. pp. 1522–1527.

Sawada, R., Hirata, K., Kitagawa, Y., Saito, E., Ueno, M., Tanizawa, K., Fukuto, J., 2021. Path following algorithm application to automatic berthing control. Journal of Marine Science and Technology 26, 541–554.

Skogestad, S., Postlethwaite, I., 2007. Multivariable feedback control: analysis and design. volume 2. Wiley New York.

Sonnenburg, C., Woolsey, C.A., 2012. An experimental comparison of two USV trajectory tracking control laws, in: 2012 Oceans, IEEE. pp. 1–10.

Yasukawa, H., Yoshimura, Y., 2015. Introduction of MMG standard method for ship maneuvering predictions. Journal of Marine Science and Technology 20, 37–52.